33rd Annual International Conference of the IEEE EMBS
Boston, Massachusetts USA, August 30 - September 3, 2011

Calibrating the Photo-thermal Response of Magneto-fluorescent Gold Nanoshells

Nrusingh C. Biswal, Ciceron Ayala-Orzoco, Naomi J. Halas and Amit Joshi

Abstract— **We report the photothermal response and Near Infrared (NIR) imaging sensitivities of magneto-fluorescent silica core gold nanocomplexes designed for molecular image guided thermal therapy of cancer. Approximately** 160 **nm Silica core gold nanoshells were designed to provide NIR fluorescent and Magnetic Resonance (MR) contrast by incorporating FDA approved dye indocyanine green (ICG) and iron-oxide within an outer silica epilayer. The imaging and therapeutic sensitivity, and the stability of fluorescence contrast for** 12 **microliters of suspension (containing approximately** 7.9 **x** 10^8 **or 1.3 femtoMole nanoshells) buried at depths of** 2-8 **mm in tissue mimicking scattering media is reported.**

I. INTRODUCTION

Silica core gold nanoshells are efficient photo-thermal therapy agents for cancer by virtue of their tunable geometry dependent Plasmon resonance which can be maximized in near infrared (NIR) region to allow photothermal heating through deep tissue [1]-[5]. Recently, we reported nanocomplexes which incorporate additional NIR fluorescence and magnetic resonance (MR) contrasts in silica core nanoshells to provide the option of fluorescence image guided photothermal therapy. In addition to their photo-thermal properties these constructs dramatically enhance (50X) the fluorescence of the only FDA cleared NIR dye: Indocyanine Green (ICG). These nanocomplexes were reported to efficiently target breast [6] and ovarian [7] cancers. To realize the promise of molecular image guided thermal therapy of cancer, we investigated the imaging stability, sensitivity, and photo-thermal response of these nanoshells at different depths in a scattering tissue like solid phantom. Section II presents the procedures for nanoshell fabrication, solid phantom preparation, photothermal treatment and fluorescence imaging set up. Photothermal treatment and fluorescence images for different concentrations of nanoshells at different depth inside the scattering medium are presented in section III. The fluorescence images of pre- and post- photothermal treated nanoshells are presented with corresponding temperature profiles. Section IV summarizes the findings.

This work was supported in part by the National Institute of Health Grant No. R01 CA 151962 (PI A. Joshi)

N.C. Biswal is with the Division of Molecular Imaging, Department of Radiology, Baylor College of Medicine, TX 77030, USA (e-mail: biswal@bcm.edu).

C. Ayala-Orzoco is with the Department of Chemistry, Rice University, Houston, TX 77005 USA (e-mail: ca5@rice.edu).

N.J. Halas is with the Department of Chemistry and the Department of Electrical and Computer Engineering, Rice University, Houston, TX 77005 USA (e-mail: halas@rice.edu).

A. Joshi is with the Department of Radiology and the Department of Molecular Physiology, Baylor College of Medicine, Houston, TX 77030, USA (Corresponding author, phone: 713-7989191, fax: 713-7988050, email:amitj@bcm.edu).

II. MATERIALS AND METHODS

A. Magneto-Fluorescent Nanocomplexes Fabrication

The nanocomplexes were fabricated similar to the procedure we previously reported with some modifications [8]. Gold nanoshells (NS) were prepared by synthesizing a metal shell of gold (15 nm layer) around a silica nanosphere (60 nm radius) giving a resonant wavelength of 770 nm [9]. At first, commercially available 10 nm Fe_3O_4 nanoparticles (Ferrotec, EMG 304) were functionalized with (3-aminopropyl) triethoxysilane (APTES, 99% purity, Sigma Aldrich). The non-functionalized Fe_3O_4 nanoparticles (100 μl) were diluted with 50 ml of H_2O, and 2 ml of APTES were added under vigorous stirring. The mixture was stirred slowly for 8 hours and then centrifuged at 1000 g for 20 minutes. The solid obtained was resuspended in 40 ml of H_2O. The amine-terminated Fe_3O_4 (500 μl) particles were added to 60 ml of NS (1x1010 particles/ml), stirred gently for 4 hours, and then centrifuged at 260 g during 15 minutes to remove excess APTES and unbound Fe_3O_4. Next the Fe_3O_4-coated NS, NS@Fe_3O_4, were coated with silica to trap the ICG fluorophore within a 10 nm silica layer. The ICG-doped silica layer was grown around the NS@Fe_3O_4 by mixing 7 ml of 1.4 x10^{10} particles/ml, 200-proof ethanol and 28% ammonium hydroxide (Fisher) in a ratio of $1 : 8.5 : 0.085$ volumes, respectively. Immediately, 5 μl of tetraethyl orthosilicate (TEOS, 99.999% purity, Sigma Aldrich) were added to the mixture under vigorous stirring. After 5 minutes, 1 ml of ICG solution in ethanol (2 mg/ml) was added, then the flask was immediately sealed and vigorously stirred during 45 minutes at room temperature. The reaction mixture was transferred to the refrigerator at 4 $^\circ C$ and was gently stirred during 3 hours to decrease the growth rate of silica layer and to facilitate the control of layer thickness. The mixture was centrifuged at 280 g for 20 minutes and the solid obtained ($NSFe_3O_4SiO_2$-ICG) was resuspended in 1 mM PBS buffer pH 7.4. The suspension was centrifuged at 300 g for 15 minutes. The supernatant was removed and the particles were resuspended once more in 1 mM PBS to give a final concentration of 6x10^{10} particles/ml and ICG concentration of 6 μM.

B. Solid Phantom Preparation

The solid phantoms were prepared with polyvinyl chloride-plastisol (PVCP) as a base material. PVCP (M-F Manufacturing Co., Fort Worth, TX, USA) is a non-toxic plastic commonly used for making fish lures and is insoluble in water. It is a white opaque solution of monomers

that polymerizes and becomes transluscent when heated to high temperatures. The opaque PVCP solution was heated in an oil bath to $\sim$ 200 $^{\circ}C$ and stirred continuously with a magnetic stirrer. The opaque grayish PVCP solution became more viscous and transluscent [10]. Once the solution reached this stage, Titanium Dioxide (TiO_2) powder (T8141, Sigma-Aldrich, USA) was added, heated and stirred continuously until the powder was homogeneously distributed in the entire solution. The solution became thick and then poured into rectangular molds and cooled over night. The reduced scattering coefficient (μ_s') of these phantoms was approximately 4.62 cm^{-1} [11].

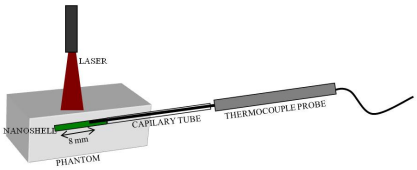

(a)

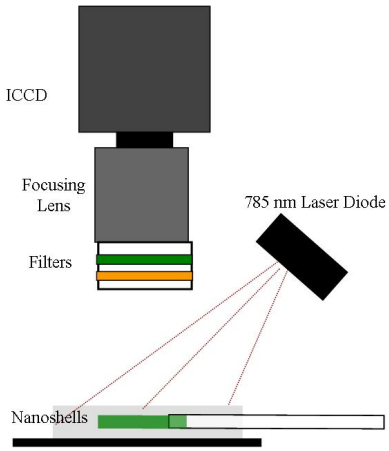

(b)

Fig. 1. Experimental setup: (a) Photothermal Treatment Setup, (b) Fluorescence Imaging Setup

C. Photothermal Treatment

The nanoshell suspension was filled in 70 mm long capillary tubes of outer and inner diameters of 1.16 mm and 1.0 mm respectively. An 808 nm laser (Diomed 15-plus, AngioDynamics, Queensbury, NY) was used to illuminate the sample and a 400 μm core 2 m long optical fiber (M32L02, Thorlabs Inc., Newton, NJ) was used to deliver light to the phantom. The laser spot size at the phantom surface was 8.0 mm. Each sample was separately exposed for 90 seconds. The temperature was monitored by a hypodermic thermocouple probe (EW-08505-92, Cole-Parmer, Vernon Hills, IL) coupled with a Digital multimeter (233, Fluke Corp.). Each capillary tube was filled with 12 μl of sample, which occupied 15 mm of the tube. As shown in figure 1 (a), only 8 mm of the filled portion of the tube was exposed with laser, which contains $\sim$ 6.4 μl sample volume.

D. Fluorescence Imaging

Pre- and post- photothermal treated samples were imaged with our home built NIR fluorescence imaging system [9]. It consists of an intensified charge coupled device (CCD) camera (Princeton Instruments, Trenton, NJ) outfitted with a 28 mm AF Nikkor lens (Nikon Inc.). The samples were excited by a 785 nm laser diode (Thorlabs Inc.). The light was diffused with a 50 mm plano-convex lens and a light shaping diffuser. A neutral density filter (OD 4) was used for capturing the excitation light images. Fluorescence images were acquired by using an 830 $\pm$ 20 nm band pass filter (Andover Corporation, Salem, NH) in combination with a holographic notch filter, OD 6 at 785 nm (Kaiser Optical Systems Inc.). A schematic of fluorescence imaging system is shown in figure 1(b). Image acquisition was controlled by customized MATLAB routines (The Mathworks Inc.) from an off-the-self personal computer (Dell Optiplex 760).

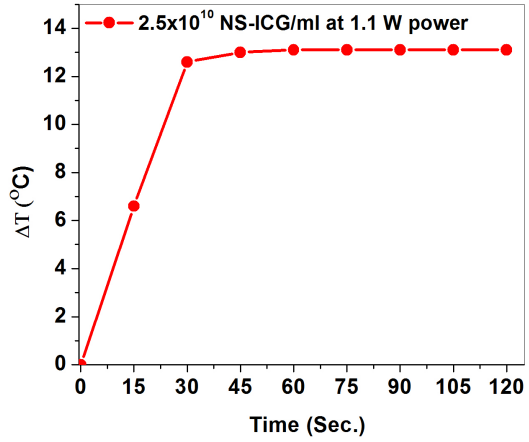

Fig. 2. Temperature profile of a tube phantom containing 2.5 x 10^{10} NS/ml illuminated at 1.1 W power for 2 minutes. Temperature reaches steady state within 1 minute.

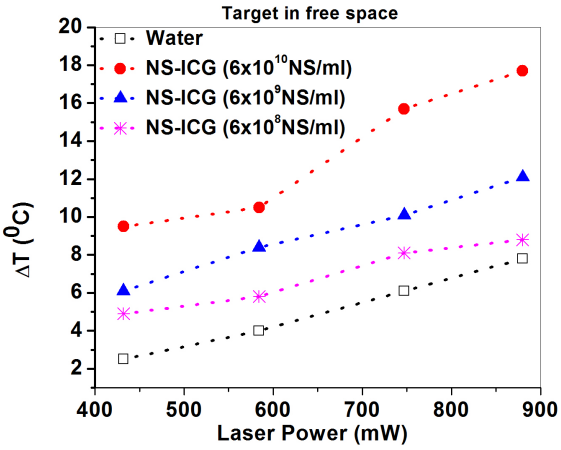

Fig. 3. Change in temperature of 6x10^{10}, 6x10^9, 6x10^8 NS/ml and water at different power for 90 seconds illumination

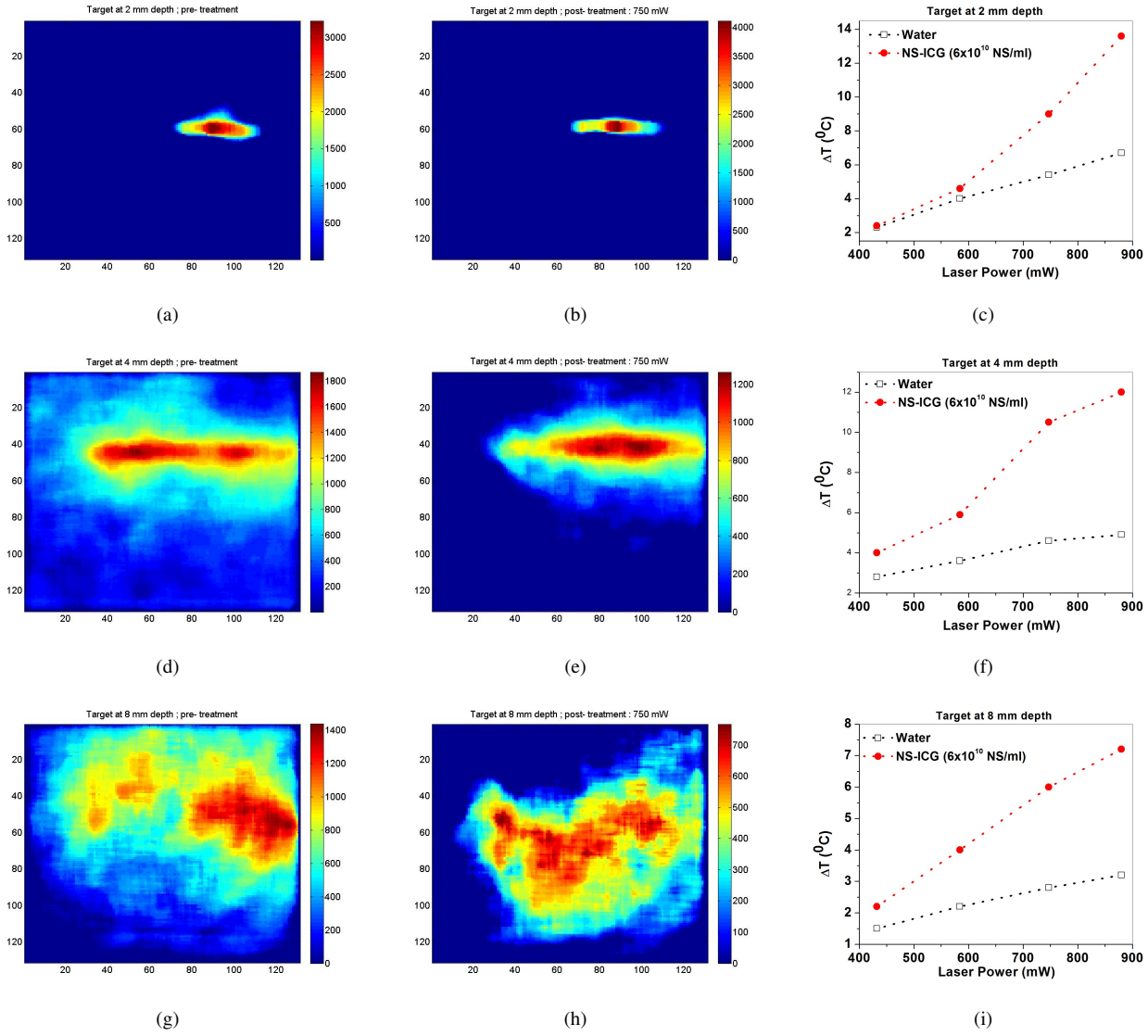

Fig. 4. (a), (d), (g) are pre-treatment fluorescence images of 6x10^{10} NS/ml at 2 mm, 4 mm and 8 mm depths respectively. (b), (e), (h) are post-treatment fluorescence images of 6x10^{10} NS/ml at 2 mm, 4 mm and 8 mm depths respectively. (c), (f), (i) are photothermal measurements from nanoshells and water at different power for 90 second illumination at 2 mm, 4 mm and 8 mm depths respectively.

III. RESULTS AND DISCUSSIONS

The first set of measurements comprised of the temperature profile with time upon NIR illumination. A capillary tube with 2.5x10^{10} NS/ml was inserted at 2 mm depth of a 10 mm thick phantom (66 mm x 45 mm). The phantom was illuminated at 1.1 W power for 2 minutes and change in temperature was monitored at 15 second intervals. As shown in figure 2, there is a step rise in temperature for the first 30 seconds then followed by a steady temperature plateau for the remaining illumination period. All the later experiments were done at 90 seconds laser exposure.

Figure 3 shows that the temperature increases with illumination power and nanoshell concentration. Temperature change from 6x10^{8} NS/ml sample was within 1-2 $^{\circ}C$ higher than that from water, and indicated the lower limit for photothermal response due to nanoshells. 6x10^{10} NS/ml concentration can provide a therapeutic temperature rise of $\sim 10^{\circ}C$.

Third set of experiments was done for 6x10^{10} NS/ml concentration sample buried at different depths inside the scattering solid phantom, and illuminated at different laser power for 90 seconds. NIR fluorescence imaging was performed pre- and post- photothermal treatment to access the robustness of fluorescence contrast to thermal damage. The pre- and post- treatment fluorescence images at different depths are shown in the columns 1&2 of figure 4 respectively. The measured temperature change (3rd column of figure 4) from nanoshells and baseline water phantom at different power and different depth show that for the power beyond 600 mW at the phantom surface, the temperature change of nanoshells increases dramatically vs water control. The fluorescence images depict increasing loss of resolution of

surface images with sample depth, which is expected due to the multiple scattering nature of phantoms. There was only a slight decrease in fluorescence emission intensity after photothermal laser illumination, indicating that the ICG encapsulated within the nanocomplexes was stable with respect to the photo-thermal heating.

IV. CONCLUSION AND FUTURE WORK

We have reported the photothermal response of magneto-fluorescent gold nanocomplexes designed for molecular imaging and thermal therapy of cancer. A $6x10^{10}$ NS/ml concentration was found to provide sufficient temperature response for therapy. The temperature increase (>7 degrees) is sufficient to induce protein degeneration in nanoshell targeted regions. As the water controls do not increase in temperature beyond 3-4 degrees under identical laser exposure, the damage to normal tissue can be minimized. [12] The integrated NIR fluorescence ability provides for tracking and labeling of cancer within deep tissue, and it can guide potential intra-operative procedures. ~ 1.3 femptomoles of nanoshells were detected within highly scattering tissue mimicking phantoms up to depth of 8-9 mm. Additionally, the fluorescence contrast was minimally affected by the photothermal heating, thus validating the potential of these constructs for image guided photothermal therapy. The imaging and therapy parameters derived from the reported studies is being applied to test the curative potential of nanocomplexes in mouse models of human breast and pancreatic cancers, as a first step toward clinical translation.

REFERENCES

[1] P. Disgaradjane et. al., Modulation of in vivo tumor radiation response via gold nanoshell-mediated vascular focused hyperthermia: Characterizing an integrated antihypoxic and localized vascular disrupting targeting strategy, *Nano Letters*, vol. 8, 2008, pp 1492-1500.

[2] S. K. Cheong, S. Krishnan, and S. H. Cho, "Modeling of plasmonic heating from individual gold nanoshells for near-infrared laser-induced thermal therapy, *Med. Phys.*, vol. 36, 2009, pp 4664-4671.

[3] N. Sharma et. al., "Depth and extent of gold nanorod photothermal conversion in tissue-mimicking phantoms," *in Proc. SPIE Photonics North*, Canada, 2010, pp. 775007.

[4] A. M. Elliott, A. M. Shetty, J. Wang, J. D. Hazle, and R. J. Staford, Use of gold nanoshells to constrain and enhance laser thermal therapy of metastatic liver tumors, *Int. J. Hyperthermia*, vol. 26, 2010, pp 434-440.

[5] G. P. Goodrich, L. Bao, K. Gill-Sharp, K. L. Sang, J. Wang, and J. D. Payne, Photothermal therapy in a murine colon cancer model using near-infrared absorbing gold nanorods, *J. Biomed. Opt.*, vol. 15, 2010, pp 018001.

[6] R. Bardhan et. al., Tracking of multimodal therapeutic nanocomplexes targeting breast cancer in vivo, *Nano Lett.*, vol. 10, 2010, pp 4920-4928.

[7] W. Chen. Et. al., A molecularly targeted theranostic probe for ovarian cancer, *Mol. Cancer Ther.*, vol. 9, 2010, pp 1028-1038.

[8] R. Bardhan et. al., Nanoshells with targeted simultaneous enhancement of magnetic and optical imaging and photothermal response, *Adv. Func. Mat.*, vol. 19, 2009, pp 3901-3909.

[9] B. E. Brinson, J. B. Lassiter, C. S. Levin, R. Bardhan, N. Mirin, and N. J. Halas, Nanoshells made easy: improving Au layer growth on nanoparticle surfaces, *Langmuir*, vol. 24, 2008, pp. 14166-14177.

[10] G. M. Spirou, A. A. Oraevsky, I. A. Vitkin, and W. M. Wgelan, Optical and acoustic properties at 1064nm of polyvinyl chloride-plastisol for use as a tissue phantom in biomedical optoacoustics, *Phys. Med. Biol.*, vol. 50, 2005, pp N141-153.

[11] R. Choe, *Diffuse optical tomography and spectroscopy of breast cancer and fetal brain*, PhD Dissertation, Department of Physics and Astronomy, University of Pennsylvania,PA, USA, 2005.

[12] H.H. Kampinga, *Thermotolerance in mammalian cells: Protein denaturation and aggregation, and stress proteins*, Journal of Cell Science, vol. 104, 1993, pp 11-17.